Numerical Methods for Integrating Nanoscale Material Features into Building Scale Energy Performance

Julian Wang

Abstract The pursuit of energy-efficient buildings has driven significant advancements in material science, particularly at the nanoscale, where materials exhibit unique optical, thermal, and mechanical properties. However, the challenge remains in effectively integrating these nanoscale features into whole-building energy performance. This chapter explores the pivotal role of numerical methods in bridging the gap between nanoscale material innovations and macroscale architectural applications. A range of computational techniques, including molecular dynamics (MD), finite element analysis (FEA), computational fluid dynamics (CFD), and machine learning-based predictive modeling, are discussed to illustrate how material properties can be accurately represented across scales. By leveraging multi-scale simulations, this research enables the translation of nanoscale behaviors—such as localized surface plasmon resonance (LSPR)-induced photothermal effects—into real-world energy performance assessments. A central case study investigates the role of plasmonic nanomaterials in spectrally selective glazing systems. The study examines how nanoparticle-induced photothermal effects enhance solar heat gain while maintaining high optical transparency, thereby improving building energy efficiency. A physics-based numerical framework is developed to model the nanoscale-to-building-scale thermal transfer, with results validated through parametric energy simulations in EnergyPlus. The findings demonstrate that LSPR-driven glazing systems can achieve heating energy savings comparable to double-pane windows while offering additional daylighting benefits. By integrating numerical modeling with real-world applications, this chapter highlights how computational methods are indispensable for optimizing advanced materials in sustainable architecture. The research underscores the necessity of multi-scale numerical simulations to unlock the full potential of nano-engineered building components, providing a pathway for bridging fundamental material science with large-scale implementation.

J. Wang (✉)
College of Engineering, Pennsylvania State University, University Park, PA, USA
e-mail: julian.wang@psu.edu
URL: https://archilambda.com

D. Shi (ed.), *Energy Materials Science and Engineering: From New Devices to AI Power Systems*, Green Energy and Technology, https://doi.org/10.1007/978-3-031-88550-1_11

Keywords Numerical modeling · Multi-scale simulation · Nanoscale materials · Building energy performance · Computational methods · Solar-responsive glazing · Photothermal effects · Parametric energy simulation

1 Introduction

The demand for energy-efficient buildings has driven extensive research into advanced building materials that can enhance energy performance. One of the most promising frontiers in this field is the integration of nanoscale materials into building applications. These materials, with their unique thermal, optical, and mechanical properties, offer transformative potential for improving insulation, thermal regulation, and overall energy efficiency. However, bridging the gap between nanoscale material discoveries and their macroscopic effects at the whole-building scale remains a significant challenge. Understanding and quantifying the impact of these nanoscale materials on building energy performance requires sophisticated numerical and simulation methods that operate across multiple scales.

1.1 Building Materials for Energy Performance Across Scales

Building materials play a crucial role in determining the energy efficiency of structures. From traditional insulation materials to innovative phase change materials (PCMs) and nanocoatings, advancements in material science have paved the way for enhanced thermal performance, reduced energy consumption, and improved occupant comfort. At the nanoscale, materials exhibit unique properties such as enhanced thermal conductivity, radiative cooling capabilities, and phase transition behaviors that can be leveraged to optimize building performance. However, the direct implementation of these nanoscale enhancements at the whole-building scale necessitates computational modeling to capture the complex interactions between materials, environmental conditions, and building operations.

Multi-scale modeling approaches have emerged as essential tools to evaluate the performance of nano-enhanced materials. These methods integrate nanoscale characteristics into macroscale simulations, allowing researchers to predict their impact on overall building energy consumption. Examples include nano-enhanced PCMs for thermal storage, nanocoatings for dynamic or spectral selective window technologies, and aerogels for superior insulation properties. Each of these applications requires rigorous computational analysis to assess their real-world effectiveness in improving energy efficiency. One of the major reasons for the necessity of these numerical and computational methods is the high cost and complexity of conducting large-scale experiments, which makes it impractical to test every material variation

physically. Additionally, uncertainties in real-world environmental conditions and material behaviors require extensive simulations to ensure accurate predictions and robust performance assessments before large-scale implementation.

1.2 The Role of Numerical and Simulation Methods

To accurately model and predict the influence of nanoscale materials on building-scale energy performance, researchers rely on various numerical and simulation techniques. These methods facilitate the translation of material properties from the atomic level to full-scale buildings, providing insights into thermal behavior, energy savings potential, and long-term durability. Molecular dynamics (MD) simulations are widely used to model the interactions of atoms and molecules within nanoscale materials, helping researchers understand thermal conductivity, phase transitions, and mechanical properties that impact building-scale applications [1, 2]. Similarly, finite element analysis (FEA) is employed to simulate heat transfer and structural integrity, allowing for the assessment of how nanoscale modifications influence building components such as walls, roofs, and windows [3]. Furthermore, computational fluid dynamics (CFD) plays a crucial role in evaluating the effects of nanocoatings and insulation materials on airflow and heat distribution within buildings. CFD simulations help optimize passive and active climate control strategies, as demonstrated in research assessing the energy performance of building windows with nanoscale photothermal effects [4]. Additionally, the co-simulated material-component-system-district framework proposed in prior work enables synthetical and comprehensive analysis of building sustainability [5].

Last, it is also worth mentioning that machine learning and physics-informed neural networks have recently emerged as powerful tools in this domain. By leveraging large datasets and predictive modeling techniques, machine learning enhances the accuracy of simulations, reducing computational costs while improving the reliability of energy performance assessments. A pertinent example is the study by Liu et al., where a hierarchical multi-scale model utilizing Physics-Informed Neural Networks (PINNs) was proposed to predict the thermal conductivity of Polyurethane incorporated with Phase Change Materials. This approach allowed for accurate predictions at both meso-scale and macro-scale levels, demonstrating the effectiveness of PINNs in modeling complex thermal behaviors in building materials [6].

1.3 Solar Responsive Nanomaterials and Glazed Façade Applications

Heating and cooling energy loss through windows represents 3.95 quads of primary energy use in the U.S. [7]. A window's thermal insulation is quantified by its U-factor; lower U-factors correspond to better insulation. The current methods for developing windows with low U-factors come from two primary directions: either structural or spectral design. From the structural design perspective, adding layers of windowpane separated by insulating barriers minimizes conductive heat transfer. However, one cannot simply add an unlimited number of thermal barriers and windowpane layers, as this would result in unacceptable transparency, haze, thickness, and other practical issues. Consequently, research has focused on addressing spectral characteristics in terms of thermal radiation and solar energy utilization. For temperatures relevant to building energy efficiency, thermal radiation flux occurs in four basic bands: ultraviolet irradiance, visible light, infrared irradiance from the sun, and longwave irradiance from interior or outdoor temperatures. About 51% of the power of solar irradiance is infrared [8], so regulating a window's spectral properties to control the passage of thermal radiation in these ranges can significantly improve building energy efficiency.

Emerging nanoscale materials and technologies play a critical role in optimizing the spectral and thermal properties of glazed façades. Innovations such as nanocoatings, spectrally selective glazing, and photothermal-responsive materials enable dynamic control over heat and light transmission. In particular, in recent years, many studies on the optical properties of nanoparticles (NPs) have found that due to the phenomenon of localized surface plasmon resonance (LSPR) [9]—the collective oscillation of conduction electrons on the surface of NPs in the presence of incident light—a few metallic NPs can show strong extinction peaks in the NIR regions of the electromagnetic spectrum. (In simple terms, they are capable of scattering or absorbing large amounts of light when illuminated.) [10–14]. It is evident that the wavelengths at which plasmonic NPs interact with light, as well as their ratio of absorption and scattering abilities, can be tuned by varying the composition, shape, and size of the particles [15–17]. These NPs are capable of manipulating light on a nanoscale with the possibility of being incorporated into spectrally selective glazing systems.

The LSPR-mediated spectrally selective behaviors have been extensively studied in recent years using both theoretical and experimental methods. Their absorption and scattering abilities and LSPR frequencies can be tuned by controlling particle size, shape, orientation, distribution, concentration, and composition [11, 15, 18]. Regarding the potential of incorporating LSPR effects into glazing structures, the most encouraging work was conducted by Milliron, which integrated the LSPR effect and electrochromism into a dynamic glazing film design, achieving 39% NIR transmission modulations with 82–85% T_{vis} [19]. Although many studies on the nanoscale have claimed that the LSPR effect can be used in building glazing systems and several conducted simple simulations or offered modest predictions [20, 21],

much less attention has been paid to analyzing the thermal and optical behaviors of the LSPR employed in complex fenestrations (e.g., with low-e coatings, air cavity, and a variety of structures). Therefore, some of the results of these attempts have **led to conflicting conclusions**, even though they addressed the same phenomenon. Studies by Li et al. [22], Xu et al. [23], Pardiñas-Blanco et al. [24], and Besteiro et al. [25] were focused on the plasmonic NPs' NIR absorption, and suggested their use in blocking solar heat for cooling purposes. Zhao et al. [26], Khashan et al. [27], and Wang and Shi [28] also focused on the NIR absorption induced by the LSPR, concluding it offered the potential for heat-related energy savings in winter. The controversy is due to the complexity of building windows' thermal and optical transfers.

In particular, highly absorptive coating schemes may block solar heat transmission, but conduct, convect, and/or radiate the absorbed energy inwards and/or outwards at relative proportions, depending on the glazing structure, low-e coating's spectral features, and positions relative to the plasmonic films, as well as the corresponding external and internal environments. Therefore, compared to the relatively established theories, models, and experimental validations in the nanomaterial field of LSPR-induced absorption and scattering, **little has changed in the physics-based numerical method** at the architectural scale that incorporates new nanoscale physical relations and models employing LSPR in the thermal and optical performances of glazing.

Although these nanoparticles have demonstrated the ability to manipulate light at the nanoscale and show promise for integration into spectrally selective glazing systems, a critical challenge remains in transitioning from fundamental material studies to practical architectural applications. The interaction of LSPR effects with multi-layer glazing system properties—such as spectral emissivity, thermal insulation, and structural placement—must be thoroughly understood through comprehensive numerical modeling and analysis. A precise evaluation of how these interactions affect the overall thermal and optical performance of glazing systems is necessary to unlock their full potential in energy-efficient building applications.

In this chapter, using the above research challenge about numerical modeling and analysis in nanoscale glazing systems as an example, the focus will be on how emerging nanoscale materials and their newly discovered physical relationships can be incorporated into building-scale performance analysis. This chapter will illustrate how advanced numerical methods can bridge the gap between fundamental nanoscale physics and practical architectural applications, demonstrating key approaches for evaluating energy transmission, spectral selectivity, and thermal efficiency in complex fenestration structures.

2 Fundamentals of the Numerical Modeling and Analysis

2.1 Thermal Transfer Modeling of Glazing Systems

Figure 1 shows the analytical glazing structures consisting of n layers; each of the layers has four key variables: $T_{f,i}$, $T_{b,i}$, $J_{f,i}$, and J_{bi}, which refer to the temperatures of the outdoor and indoor-facing surfaces, and radiant heat fluxes leaving the front and back-facing surfaces, respectively.

The heat flux across the ith gap (q_i) is

$$q_i = h_{c,j}\left(T_{f,j} - T_{b,j-1}\right) + J_{f,j} - J_{b,j-1} \tag{1}$$

Similarly, the heat flux across the $(i+1)$th gap is

$$q_{i+1} = h_{c,j+1}(T_{f,j+1} - T_{b,j}) + J_{f,j+1} - J_{b,j} \tag{2}$$

The solution (i.e., the temperature at each glazing surface and corresponding radiant fluxes) is generated by applying the following four equations at each layer:

$$q_i = S_i + q_{i+1} \tag{3}$$

$$J_{f,j} = \varepsilon_{f,j}\,\sigma T_{f,j}^4 + \tau_i J_{f,j+1} + \rho_{f,j} J_{b,j-1} \tag{4}$$

$$J_{b,j} = \varepsilon_{b,j}\,\sigma T_{b,j}^4 + \tau_i J_{b,j-1} + \rho_{b,j} J_{f,j+1} \tag{5}$$

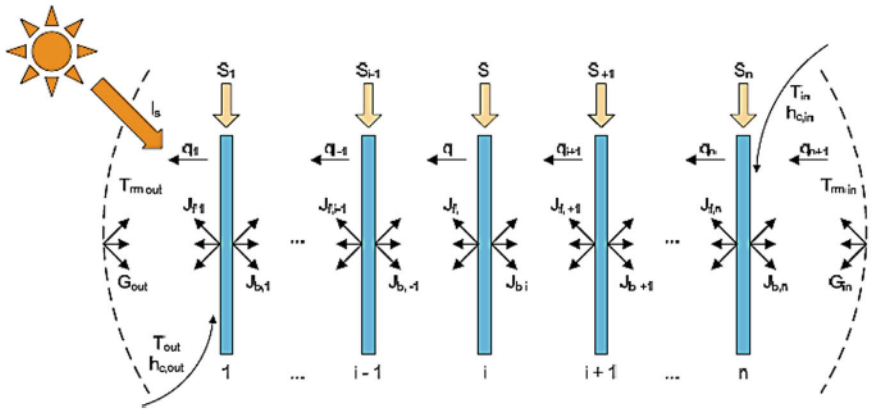

Fig. 1 Numbering system, boundary conditions and energy balance for N-layer glazing system

$$T_{b,j} - T_{f,j} = \frac{t_{g,j}}{2k_{g,j}}[2q_{i+1} + S_i] \tag{6}$$

Equation 3 describes the energy balance imposed on the surface of the *i*th glazing layer. Equations 4 and 5 define the radiosity at the *i*th glazing, where $\rho_{f,j} = 1-\varepsilon_{f,j}-\tau_i$ and $\rho_{b,j} = 1 - \varepsilon_{b,j} - \tau_i$, while the temperature difference across the *i*th glazing layer is given by Eq. 6. In all, four *n*-equations can be written for a glazing system; these can either be solved using an iterative solution algorithm with convergence checking on the sets of glazing-layer temperatures [29, 30], or by setting equations in matrix form and then decomposing the matrix to find sets of glazing-layer temperatures [31, 32]. In response to such basic methods, some studies have focused on improving the analytical models, including correcting the convective heat coefficient [33, 34], and internal shading effect models [35], conjugating the heat transfer analysis after considering both the conduction and convection processes [36], and comparing empirical correlations to long-wave reflectivity [37].

Within a macroscopic framework, a temperature field is assumed not only to be a continuum, but also to hold a thermal equilibrium at every location [38, 39]. Conventional window heat transfer studies are built upon such assumptions [40]. However, when the thickness scale is comparable to or smaller than the mean free path of the material, the macroscopic model is of question [41 –44]. Since there are no sufficient energy carriers in the interested direction, the temperature field is discontinuous. Once the concept of a temperature gradient fails, the classic Fourier's law is also questionable, as is the associated diffusion equation. A similar situation exists in the response time for temperature [45, 46]. The macroscopic heat equation assumes that the temperature gradient follows simultaneously with the heat flux vector [38]. Due to the quick thermal effects activated by the LSPR, the response time of primary concern is of the same order of magnitude as the mean free time; the lagging behavior caused by phonon–electron interaction in films or phonon scattering must be taken into account [47, 48]. On the nanoscale, some models analyzing thermal behaviors that are strongly enhanced in the presence of plasmonic NPs have been developed and experimentally verified [46–49], but little research has studied the micro-to-macroscale heat transfer mechanism of multi-layer glazing structures with air layer and low-e coatings.

2.2 *Spectral Solar Irradiance Modeling*

Accurate knowledge of locally available solar radiation is essential for the proper sizing, design, and dynamic simulation of solar energy systems [50]. Initial approaches used current weather conditions as input for mathematical models with dynamic atmosphere parameters and solar physics to predict global solar irradiance [51–53]. The typical meteorological year (TMY) data files, developed from extensive datasets, serve as the most widely used weather files in building envelope simulations. Each TMY file consists of 12 months selected as most representative of

long-term climate patterns. These files include three primary broadband solar components: global horizontal irradiance (GHI), direct normal irradiance (DNI), and diffuse horizontal irradiance (DHI). These components encompass ultraviolet (UV), visible light (VIS), and near-infrared radiation (NIR), which are critical for solar energy and building performance simulations.

Recent research has highlighted the necessity of decomposing broadband solar radiation into narrowband components or specific spectral bands for more accurate analyses. Solar VIS radiation can enhance indoor lighting efficiency and circadian health [54] but also causes glare issues. NIR radiation can reduce heating loads in cold climates but is undesirable in hot regions. Additionally, studies have shown that VIS and NIR transmission through glazing affect occupants' thermal comfort differently near windows [55]. With the advent of spectral-selective materials, independent modulation of solar radiation across different spectral bands has become feasible. For instance, metallic nanoparticle-based nanocomposites leverage plasmonic resonance effects to selectively modulate VIS and NIR transmission. Jahid et al. demonstrated reversible photothermal windows utilizing nanoscale solar-induced plasmonic photothermal effects to regulate solar heat independent of visible light conditions [56, 57]. Shen et al. explored silver nanorods (AgNRs) that allow for over 50% luminous transmittance while blocking up to 80% of solar radiation via tunable plasmonic resonance [58]. Forrest et al. reviewed semitransparent organic photovoltaics, which selectively absorbs UV and NIR while maintaining visible transparency, making them ideal for power-generating windows [59]. Other researchers have also investigated light and heat-splitting materials by designing spectral transmittance and absorptance properties of glazing materials across different solar spectra [25, 60–62].

To assess photovoltaic systems and solar-selective glazing that incorporate nanoscale spectral-selective features, several solar decomposition models—such as the BRL, Perez, Boland, Maxwell, and Lauret models—have been developed to predict spectral irradiance from broadband global radiation using statistical techniques. However, accurately modeling visible and NIR components for the glazing surface remains essential for optimizing NIR-modulated window systems. Due to the high cost of spectroradiometers, most regions lack direct measurements of spectral components, relying instead on pyranometer-derived broadband data. As a result, many conventional weather files lack spectral information needed for precise simulation of spectral-selective materials.

To address this gap, a reconstruction algorithm is needed to decompose solar VIS and NIR irradiance from broadband radiation data for building simulations. Given that solar simulation relies on GHI, DHI, and DNI components, all three must be decomposed into narrowband data. We have conducted two specific studies to develop models for decomposing broadband solar irradiance data into its visible (VIS) and near-infrared (NIR) components. The first study focused on developing a predictive model using the Classification and Regression Tree (CART) algorithm for estimating VIS and NIR components in global horizontal irradiance (GHI) based on typical meteorological year (TMY) weather data. The second study extended the above-mentioned work by building spectral solar radiation models for direct normal irradiance (DNI) and diffuse horizontal irradiance (DHI), using extracted and derived

features from existing weather files without requiring additional measurements or sensor installations.

(1) Decomposing VIS and NIR from GHI

The model development utilized two years of solar spectral and TMY-compliant hourly weather data from the Solar Radiation Research Laboratory (SRRL) Baseline Measurement System (BMS) database at NREL. The dataset, covering wavelengths from 300 to 1700 nm, underwent rigorous data cleaning, including the removal of missing, outliers, and erroneous values based on physics-based calculations. After processing, the finalized dataset consisted of 7,583 observations. To enhance model generalizability across different locations, we incorporated ten local meteorological parameters, such as humidity and temperature, along with five newly derived predictor variables informed by solar radiation and building physics principles. Among these, the cloud transmittance parameter, derived from cloudiness values in standard weather files, was particularly effective in improving model accuracy for the NIR component. In total, 15 predictor variables were used to develop the estimation models for hourly VIS/GHI and NIR/GHI. Model validation yielded strong results, with mean absolute error (MAE) between 2.13 and 2.41% and root mean square error (RMSE) between 3.88 and 4.25%, confirming the reliability of the classification tree models [63].

(2) Decomposing VIS and NIR from DNI and DHI

For DNI and DHI components, we employed an extreme boosting regression tree method, leveraging readily available TMY weather data. Multiple databases from the NREL Solar Radiation Research Laboratory were curated and processed [64]. After a thorough data cleaning procedure, which involved removing missing values, outliers, and physically erroneous data, the finalized dataset comprised 11,862 observations. To ensure the model's generalizability across different locations, easily obtainable meteorological parameters were incorporated into the modeling process. The full estimation model utilized 20 predictive variables, while a simplified version, designed for scenarios with limited meteorological data, relied on 15 predictive variables.

Four widely used supervised, non-parametric machine learning algorithms—Decision Tree, M5' Tree, Random Forest, and XGBoost—were employed to train and compare the models. The comparative analysis revealed that XGBoost outperformed the other techniques in accuracy and reliability for DNI decomposition across both full and simplified models. It achieved the lowest RMSE (18.080 for V1, 18.985 for V2, 15.868 for N1, and 17.606 for N2) and MAE (9.192 for V1, 10.181 for V2, 8.383 for N1, and 9.506 for N2), along with the highest R^2 values (0.983 for V1, 0.980 for V2, 0.993 for N1, and 0.990 for N2). Among the predictive variables, DNI and Kb were identified as the most influential for both VIS and NIR decomposition. Additionally, certain atmospheric parameters, including aerosol optical depth (AOD), precipitable water vapor (PWV), and total and opaque sky cover, contributed significantly to the predictions. Through feature importance and interaction analyses, previously hidden correlations between predictors, as well as between predictors and responses, were uncovered.

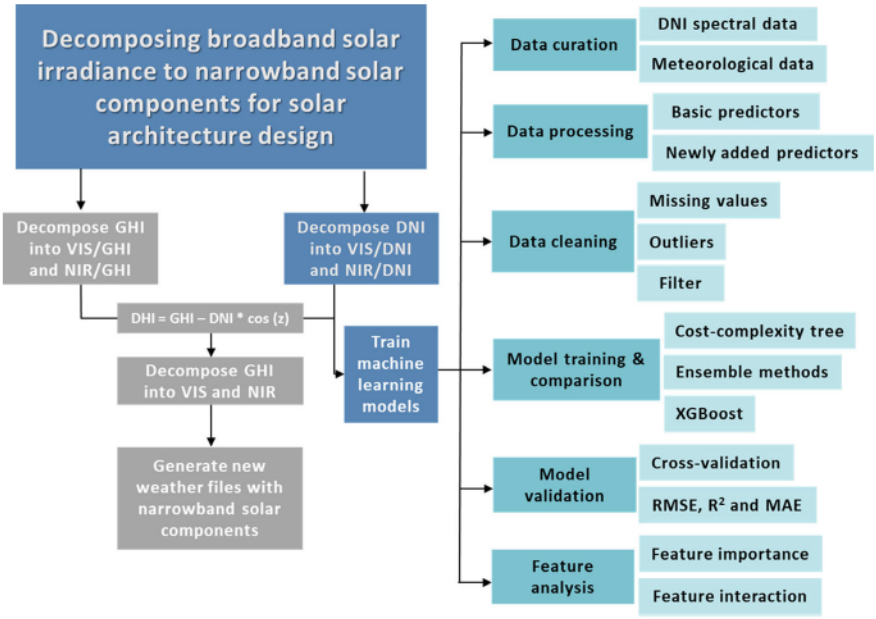

Fig. 2 The workflow of generating new weather files with narrowband solar components

By leveraging the above two models, it becomes feasible to effectively break down conventional, broad-spectrum weather files into distinct, narrowband weather files. Figure 2 presents the workflow of generating new weather files with narrowband solar components. Subsequently, this can be fed into typical building energy simulation programs for further analysis of integrating nanoscale spectral selective materials into building scale.

2.3 Parametric Energy Simulation and Performance Analysis

Parametric energy simulation is different from the traditional energy simulation procedure and incorporates more complicated parametric relationships between the design variables, construction states, and environmental boundaries. The original development of the overall workflow of parametric energy simulation was for dynamic building envelope's performance simulation. Throughout the history of architecture, dynamic building envelopes have attracted tremendous attention and effort due to their aesthetic characteristics, pleasant visual impact, design uniqueness, and interaction with users [65–67]. The dynamic envelope concept has long been established and integrated into the current architecture curriculum via a variety of generative design tools and fabrication techniques [68–70]. Nevertheless, until recently, advances in and the availability of new materials and structures such as

vacuum insulation [71, 72] and gas-filled panels [73, 74]; phase-change materials [75, 76]; and thermotropic, photochromic, and electrochromic materials have focused the attention of architects and designers on such envelopes' performance [77–79]. One of the fundamental steps in establishing performance-driven dynamic envelopes is an analytical approach that determines the range of dynamic properties necessary to satisfy the adaptability requirements, as well as their amplitude of variability. Since the development of this kind of analysis requires a "parametric energy" approach (i.e., environmental conditions and envelope behaviors must be parametrically connected), the simulation instruments currently available are often inadequate; thus, researchers must develop ad hoc numerical models [80] (such as the CABS approach) for wall-specific heat and thermal conductivity [81, 82], external absorption coefficients of the surface, glazing typologies, the sensitivity analysis framework for the envelope's thermal properties [83–85], and the BKE method for the envelope's thermal conductivity and SHGC [80, 86–88]. To integrate the new dynamic structures into glazing systems (e.g., LSPR-mediated dynamic attachments), a computationally efficient method is needed to quantitatively ideate and optimize the characteristics of a system.

Here we introduce the parametric energy simulation method and procedure utilizing the Energy Management System (EMS) in EnergyPlus. EnergyPlus is a widely used, open-source building energy simulation engine developed by the U.S. Department of Energy (DOE). It enables the modeling of energy consumption for heating, cooling, ventilation, lighting, and other building-related processes. EnergyPlus EMS module is particularly advantageous for integrating advanced simulation techniques, such as parametric energy modeling, to account for complex, dynamic physical relationships not inherently embedded in conventional building simulations. The EMS-based parametric energy simulation method allows users to define custom control algorithms and dynamic parameter adjustments, making it ideal for advanced energy modeling scenarios. Similar EMS-based approaches have been applied in previous studies to incorporate dynamic parameters into energy simulations [87, 89–96].

An EMS program in EnergyPlus comprises several essential components:

- **Sensor**—Extracts information from the model (e.g., temperature, humidity, solar radiation).
- **Actuator**—Modifies specific model components or elements based on sensor input.
- **Program Calling Manager**—Determines when the EMS program is executed.
- **Program**—Defines the logic for modifying model parameters using conditional statements.
- **Construction Index Variable**—Links EMS-based changes to material properties within the simulation.

In particular, sensors in EnergyPlus can be used to track key environmental parameters relevant to window technology simulations, such as indoor air temperature, relative humidity, and incident solar radiation. The actuator then modifies window properties based on these sensor readings, allowing for dynamic adjustments in response to external conditions. For example, if window properties vary

based on outdoor temperature, the EMS sensor should monitor "Site Outdoor Air Drybulb Temperature," while the actuator should control "Construction State" to modify the window properties dynamically. The Program Calling Manager should be set to "Begin Timestep Before Prediction," ensuring that adjustments occur before EnergyPlus predicts energy performance for the next timestep. The program logic is implemented using "IF" statements and "While" loops, allowing windows to respond dynamically to changing outdoor air temperature conditions.

A crucial advantage of EMS-based parametric simulations is the ability to bridge the gap between nanoscale material properties and large-scale building energy performance. Parametric relationships can be derived from: experimental data on advanced glazing systems incorporating nanomaterials; regression models based on numerical simulations of nanoscale materials. Using the "Construction Index Variable" section in EnergyPlus, optical and thermal properties of an advanced glazing system are linked to the EMS program. These properties are defined under the "Window Material: Glazing" section and are dynamically adjusted based on the assigned outdoor weather conditions in the EMS Program section.

The following diagram outlines the workflow for implementing an EMS-based parametric energy simulation, demonstrating how advanced parametric relationships are incorporated into building-scale energy analysis:

- **Define sensors** to extract real-time weather and indoor environmental data.
- **Select actuators** to modify dynamic material or system properties.
- **Develop EMS logic** using conditional programming to enable real-time responsiveness.
- **Integrate nanoscale material properties** by linking EMS with advanced material simulations.
- **Run parametric simulations** in EnergyPlus to evaluate energy performance.

This EMS-based approach enhances the accuracy of building energy simulations by integrating real-time, complicated physical relationships, particularly for new glazing systems and other advanced building envelope technologies that incorporate newly discovered nanoscale materials and features (Fig. 3).

3 Case Study: Numerical Analysis of the Energy Performance of Solar NIR-Driven Nano Plasmonic Photothermal Effects

3.1 Theoretical Analysis and Physical Relationship Derivation from Experiments

The overall heat transfer process under solar radiation is illustrated in Fig. 4. For building windows, solar radiation is transmitted, absorbed, and reflected in varying proportions based on the window's optical properties and environmental conditions.

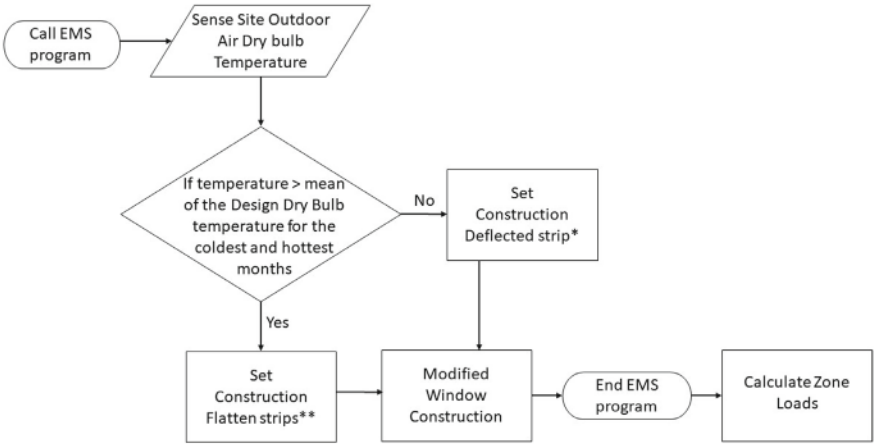

Fig. 3 Exemplary EMS workflow at each timestep for yearly energy use simulation [97]

Transmitted solar radiation directly reduces space heating demands, while absorbed radiation partially flows inward from the panes, increasing indoor temperatures and enhancing heating energy savings in winter. The distribution of these effects is quantified by the solar heat gain coefficient (SHGC) in fenestration analysis. The absorbed solar irradiance (q_{abs}) was calculated by Eq. 7. Similarly, the solar irradiance (q_{trans}) transmitted by the glazing system was obtained by Eq. 8. Solar irradiance can increase the glazing system's temperature, especially in photothermal windows.

$$q_{\text{abs}} = \int G_\lambda \alpha_\lambda d_\lambda \tag{7}$$

$$q_{\text{trans}} = \int G_\lambda \tau_\lambda d_\lambda \tag{8}$$

where G_λ is the incident spectral irradiance from solar light or simulated solar light and α_λ is the spectral absorptance of the photothermal-coated windows.

The solar energy absorbed by a glazing system contributes to a spontaneous temperature rise in the glazing. In a conventional steady-state heat transfer model, this temperature change is governed by

$$\frac{\mathrm{d}T}{\mathrm{d}t} = \frac{1}{c * m} * \left(\sum Q_{\text{in}} - \sum Q_{\text{out}}\right) \tag{9}$$

$$Q_{\text{in}} = q_{\text{abs}} * A_s \tag{10}$$

$$Q_{\text{out}} = Q_{\text{conv}} + Q_{\text{cond}} + Q_{\text{rad}} \tag{11}$$

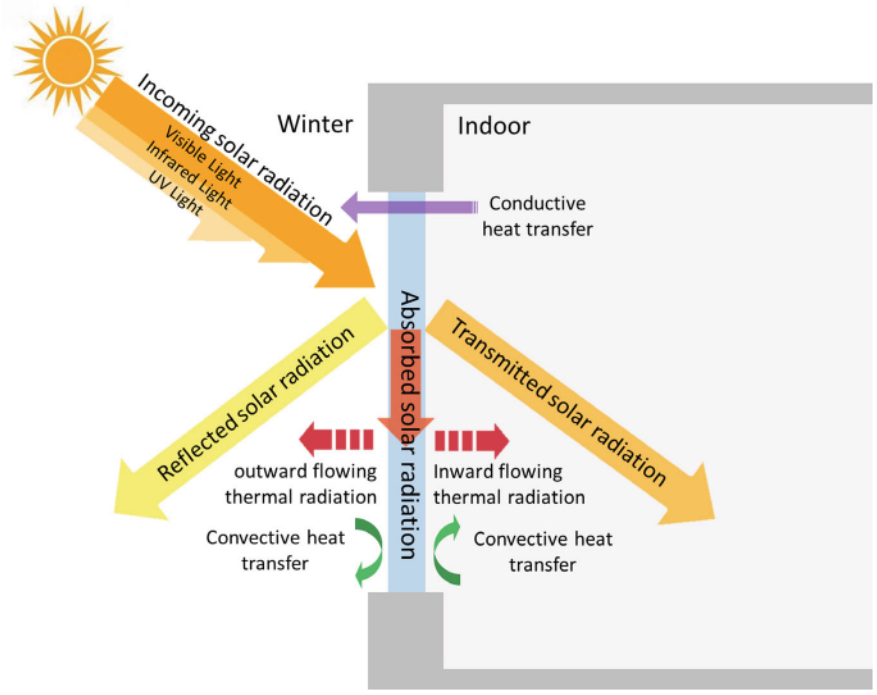

Fig. 4 Solar radiation and window thermal transfer

Here, c is the heat capacity (J/g K), and m is the material mass (g). Under predefined internal and external boundary conditions, Q_{in} corresponds to the absorbed solar radiation on the window surface (Eq. 10), while Q_{out} accounts for conductive, convective, and radiative heat transfer from the glazing's interior and exterior surfaces (Eq. 11). This process is complex due to convection flow and surface emissivity variations. With stable ambient air conditions and continuous solar irradiance, an energy balance model can be developed to analyze thermal behavior and temperature distribution. Traditional calculations assume the glazing system as a homogeneous bulk, leading to an equal temperature rise on both surfaces.

However, as highlighted in the introduction, when plasmonic NPs coat the glazing surface, LSPR-induced photothermal effects can significantly elevate the coating surface temperature while reducing heat transfer to the substrate. This phenomenon is attributed to a quasi-ballistic effect, where the NP size is much smaller than the phonon mean free path in the substrate material [98]. Inspired by previous studies on LSPR-induced solar vapor generation [99], an interfacial insulation layer (R_h) was hypothesized between the NP-coated layer and the glazing substrate [57]. This layer was incorporated into the conventional heat transfer model to account for heat dissipation variations.

Under stable boundary conditions and identical ambient temperatures, the absorbed solar energy Q_{in} is dissipated through the NP-coated surface and via conductive transfer through the interfacial layer into the glass. The heat dissipation Q_{out} is expressed as

$$Q_{\text{out}} = h_{\text{con-NP}}(T_{\text{NP},s} - T_{\infty}) + A_s + \varepsilon_{\text{NP}}\sigma(T_{\text{NP},s}^4 - T_{\infty}^4)A_s + \left(\frac{1}{R_h}\right)(T_{\text{NP},s} - T_{\text{glass},s})A_s \quad (12)$$

where

- $T_{\text{NP},s}$ is the coating surface temperature.
- $T_{\text{glass},s}$ is the soda-lime glass surface temperature.
- $(T_{\text{NP},s} - T_{\text{glass},s})$ represents the temperature differential across the interfacial insulation.
- T_{∞} is the ambient temperature.
- R_h is determined by fitting the analytical surface temperature model to measured data.
- $h_{\text{con-NP}}$, ε_{NP}, σ are heat transfer parameters specific to the photothermal coating.

Notably, unlike conventional macroscopic heat transfer models that are used in building scale heat transfer and energy balance calculations, this function assumes the interfacial insulation layer acts as a thermal barrier, moderating heat transfer from the NP layer to the glass while enhancing heat dissipation at the coating surface. By integrating Eqs. (9–12), the two-dimensional temperature evolution from initial irradiation to steady-state conditions can be analytically solved.

The key hypothesized interfacial insulation R_h needs to be obtained through nanoscale material experiments. In this case study, $Fe_3O_4@Cu_{2-x}S$ was particularly selected, which has been found to have robust spectrally selective absorption of NIR radiation with only a minor reduction in the visible region. The material demonstrates highly efficient photothermal heating conversion under continuous illumination at room temperature. The synthesis and fundamental characterization of $Fe_3O_4@Cu_{2-x}S$ photothermal nanoparticles (NPs) have been previously reported [100]. They revealed that the absorption peak of $Fe_3O_4@Cu_{2-x}S$ NPs shifts from 960 nm to 1,150 nm as particle size increases from sub-10 to 15 nm. Based on this, $Fe_3O_4@Cu_{2-x}S$ NPs with an average size of 15 nm were synthesized and utilized in this study.

The NP solutions were spin-coated onto glass panes ($\sim$2.5 $\times$ 2.5 cm^2) for 10 s at 1,000 rpm, with varying concentrations. The resulting thin-film NP mass per unit coating area was 2.54×10^{-4} g/cm^2. The spectral properties, including transmissivity and reflectivity, were measured using a LAMBDA 900 UV/Vis/NIR spectrophotometer (Fig. 5b). The coated samples were exposed to an irradiance of 1,000 W/m^2 using a Newport 150W solar simulator, while the surface temperature was continuously monitored with a FLIR E6 infrared camera. Nanoscale materials experimental results indicate that the surface temperature of the $Fe_3O_4@Cu_{2-x}S$ NP-coated glass

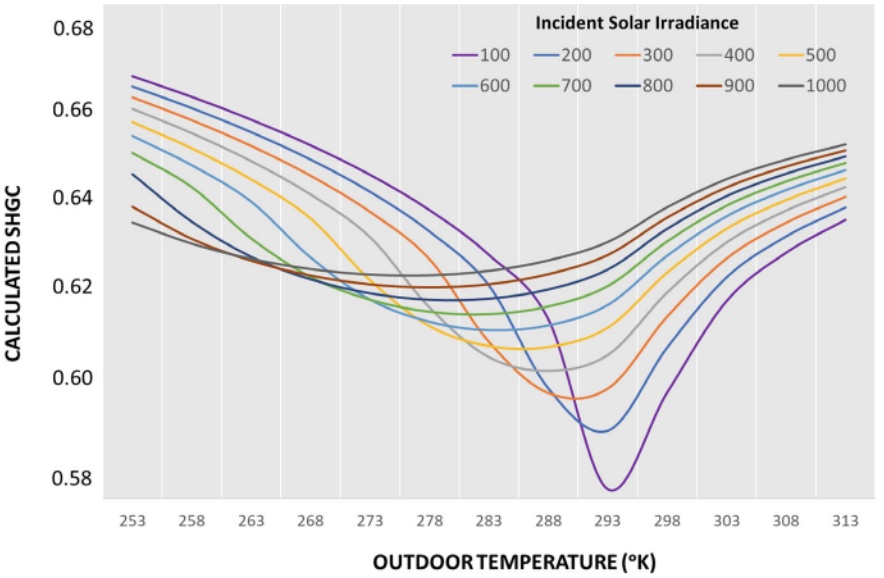

Fig. 5 SHGC variations driven by nanoscale PPE with different outdoor boundaries

increased rapidly under simulated solar radiation, reaching a thermal equilibrium within 10 min. Upon turning off the solar simulator at the 10-min mark, temperature decay was monitored throughout the cooling period.

As mentioned above, the presence of the interfacial insulation was assumed to match the enhanced temperature rise by the nanoscale plasmonic photothermal effect (PPE). By fitting the analytically calculated surface temperature to the measured data above, $R_h = 0.03$ m^{2}K/W was obtained. In other words, a thermal barrier appears when it comes to the surface plasmonic resonance of the Fe_3O_4@$Cu_{2-x}S$ NPs and reduces the effective thermal conductance to another side of the glazing. Notably, such interfacial insulating ability is only activated when solar radiation is incident on the materials.

3.2 Influence of Nanoscale PPE on SHGC

In conventional photothermal processes, the temperature rise of building glazing systems increases with higher absorbed solar energy. However, the fraction of thermal energy transferred indoors may be reduced by the low emissivity of the inner surface. According to the NFRC SHGC calculation standard, the Solar Heat Gain Coefficient (SHGC) is defined as:

$$\mathrm{SHGC} = \tau_s + N_i \alpha_s \tag{13}$$

where τ_s is the solar transmittance of window systems, α_s is the solar absorptance, and N_i is the inward-flowing fraction of absorbed radiation.

The value of N_i is influenced by the heat transfer coefficients on the glazing's inner and outer surfaces. When solar absorptance is low, the inward-flowing heat fraction remains minimal, particularly when the inner surface has low emissivity. Under such conditions, boundary conditions have little to no impact on the SHGC. However, for high solar absorptance scenarios, boundary conditions can significantly alter N_i. Moreover, the temperature increase in this study is not solely attributed to increased photon absorption but also to the strong LSPR-induced plasmonic heating effect. The LSPR-induced PPE is governed by the electric field intensity generated by the collective oscillation of energetic electrons upon resonant excitation. At higher irradiation intensities, a greater number of energetic electrons are excited within the plasmonic NPs, leading to an enhanced PPE.

The mathematical model developed in Sect. 3.1 was used to examine the relationship between solar irradiance levels, PPE effects, and the inward-flowing fraction of absorbed solar radiation under varying outdoor air temperatures. Solar irradiance levels ranging from 100 to 1,000 W/m^2 were selected to represent the incident radiation on a vertical window surface. The outdoor temperature varied between 258 and 313 K in 5 K increments, while the indoor temperature remained constant at 297 K. This setup resulted in 130 different boundary condition combinations.

Using the analytical model, temperature distributions across window surfaces were determined, followed by the calculation of inward-flowing thermal radiation, inward-flowing fraction, and SHGC. These calculations adhered to the NFRC 201 solar calorimetric method, as described by the following equations:

$$Q_{\text{solar gains}} = h_i A_s (T_{\text{in},s} - T_i) + \varepsilon_i \sigma A_s (T_{\text{in},s}^4 - T_i^4) \tag{14}$$

$$\text{SHGC} = (Q_{\text{solar gains}} - Q_{\text{U-factor}}) / \int A_s G_\lambda \tag{15}$$

where $Q_{\text{solar gains}}$ is the overall heat flux flowing through the window under solar irradiation and given temperature boundaries, $T_{\text{in},s}$ is the inner surface temperature of the window, T_i represents the indoor air temperature, and T_∞ is the ambient air temperature. h_i, ε_i, k_{in}, σ are parameters or constants involved in the convective and radiative heat transfer. $Q_{\text{U-factor}}$ is the heat flux due to indoor and outdoor air temperature differences and calculated upon the overall U-factor of the window system. G_λ is the spectral solar irradiance incident on the window. To simplify the analysis, the effects of incident solar angles, window frames, glazing edges, and condensation were not considered.

The SHGC variations of the window with nanoscale PPE are complicated. This feature can be clearly seen in Fig. 5. Since solar transmittance remained constant across all conditions, variations in SHGC were primarily influenced by changes in the inward-flowing heat fraction. Theoretically, when the temperature difference between the inner window surface and indoor air is minimal, the inward-flowing

heat fraction is negligible, resulting in the lowest SHGC value. For example, at an incident solar irradiance of 100 W/m^2, the inner window surface temperature reached 297.6 K when the outdoor temperature was approximately 293 K, yielding a minimum SHGC of 0.58. Conversely, when the temperature increase caused by 100 W/m^2 solar irradiation brought the outer window surface temperature closer to the outdoor conditions, the SHGC reached its maximum value of 0.67. Furthermore, since SHGC variations are driven by changes in inward-flowing heat rather than solar transmittance, the visible transmittance of the photothermal windows remains unaffected.

3.3 *Parametric Energy Simulation with Nanoscale PPE-Driven SHGC*

Although such SHGC variations with the nanoscale PPE observed in Sect. 3.2 are complicated, it can be integrated into the building simulation program via the EMS module of EnergyPlus. To integrate this dynamic SHGC into an energy simulation platform for analyzing photothermal windows, a simplified mathematical model is necessary. Given the data distribution and physical significance of SHGC, a parabolic function of the form $y = a(x - b)^2 + c$ as used to model SHGC for the photothermal window.

In this model, parameter b represents the outdoor temperature at which y equals c, corresponding to the minimum SHGC. The final regression model is expressed in Eq. 16. To distinguish this from the standard SHGC concept, we introduce the term $\mathrm{SHGC_{PPE}}$, which specifically accounts for the nanoscale PPE-induced solar heat gain characteristics.

$$\mathrm{SHGC_{PPE}} = a(T_o - b)^2 + c \tag{16}$$

$$a = 4.5 \times 10^{-5}$$

$$b = -0.02 \times \int G_\lambda \mathrm{d}\lambda + 297.17$$

$$c = 4.13 \times 10^{-5} \times \int G_\lambda \mathrm{d}\lambda + 0.58$$

where $\int G_\lambda \mathrm{d}\lambda$ is the total incident solar irradiance and T_o is the outdoor temperature. This model can be simply interpreted from the physical perspective and also estimate the photothermal window SHGC with high accuracy (mean absolute percentage error 1.7%, root mean square error 0.01).

Furthermore, to evaluate whole-building energy performance while accounting for the dynamic characteristics of $\mathrm{SHGC_{PPE}}$, the parametric energy simulation approach described in Sect. 2.3 was required to model the evolving properties of building

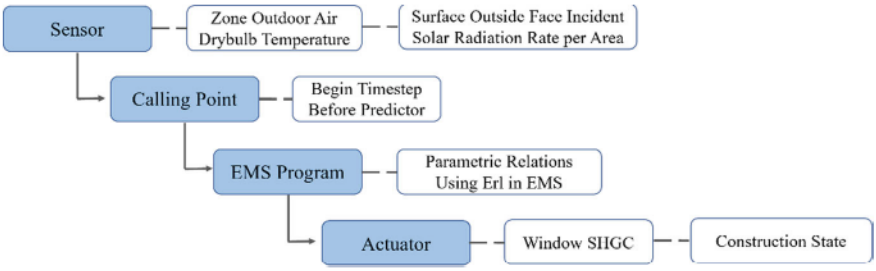

Fig. 6 EMS parametric energy simulation workflow for windows with nanoscale PPE

windows. In this simulation, the following parameters were selected as sensors: "Zone Outdoor Air Dry Bulb Temperature" (to track external temperature conditions) and "Surface Outside Face Incident Solar Radiation Rate per Area" (to capture solar irradiance on window surfaces). The actuator used was "Construction State," which determines the window type and its associated properties. Regarding the simulation workflow, the EMS calling point "Begin Timestep Before Predictor" was used, ensuring calculations occurred at the start of each timestep, before zone loads were determined. The $SHGC_{PPE}$ model (Eq. 16) was implemented to dynamically compute SHGC values for different window configurations. The parametric energy simulation workflow incorporating $SHGC_{PPE}$ is illustrated in Fig. 6.

The DOE prototypical small office building model (single-story, ~510 m^2 floor area) was selected as the case study, following the most recent ASHRAE 90.1 standards. The window-to-wall ratio was approximately 24.4% on the south-facing façade and 19.8% on the other three orientations. In this model, windows were the only control variable, allowing for a focused analysis of photothermal window performance. To evaluate energy performance, the windows with nanoscale PPE were compared against three conventional window types: Single-pane clear windows, Single-pane low-e coated windows, and Double-pane windows. The thermal and optical properties of each window type used in this analysis are detailed in Table 1. The construction configurations for single-pane clear, single-pane low-e, single-pane photothermal, and double-pane windows were implemented in EnergyPlus, replacing the original windows in the prototypical model. To ensure a fair performance comparison, all other building components—including roofs, walls, lighting, and HVAC system configurations—were kept identical across all simulations.

The prototypical model was designed with a core zone and four perimeter zones, one for each cardinal direction. A series of annual whole-building energy simulations were conducted across four climate zones (Zones 3–6). Representative cities selected for each climate zone included: Atlanta, GA (Zone 3), Seattle, WA (Zone 4), Chicago, IL (Zone 5), and Great Falls, MT (Zone 6).

Additionally, given the potential risk of overheating associated with photothermal windows, an additional design modification was introduced. Fixed overhangs were added to the photothermal window models to mitigate excess solar heat gain during summer. The depth of these overhangs was determined based on solar angles during

Table 1 Window properties used in whole building energy analysis

Window	U-factor (W/Km^2)	Solar heat gain coefficient	Visible transmittance	Emissivity
Single-pane clear	5.88	0.87	0.90	0.84 (surface 2)
Single-pane low-e	3.28	0.55	0.76	0.05 (surface 2)
Single-pane photothermal	3.30	0.58–0.67	0.75	0.06 (surface 2)
Double-pane low-e	2.42	0.53	0.68	0.05 (surface 3)

the summer solstice for each representative city, ensuring an optimized balance between winter solar gain and summer shading. This setup allowed for a comprehensive comparison of photothermal window performance across different climatic conditions while addressing potential thermal comfort concerns.

3.4 Whole Building's Energy Analysis

Since the case study in this chapter was designed and developed for heating energy saving purposes, this section presents the heating loads energy at the whole building scale particularly. The energy use of a single-pane clear window was established as the baseline for comparison. Annual energy savings percentages were calculated for single-pane low-e, single-pane photothermal, and double-pane windows relative to this baseline. The annual heating loads and corresponding energy savings across the four studied cities are presented in Fig. 7. The addition of a low-e coating led to 3.3–11.9% annual heating energy savings compared to single-pane clear windows. This improvement is primarily attributed to enhanced thermal insulation, though it also results in some reduction in solar heat gain due to the low-e coating's reflective properties. In contrast, the designed windows with nanoscale PPE exhibited significantly greater heating energy savings in winter, achieving 16.2–20.8% reductions relative to the baseline model. Compared to single-pane low-e windows, the photothermal systems provided an additional 7.6–13.2% heating energy savings due to their enhanced nanoscale PPE-induced heat gain.

The previously mentioned heating energy savings were calculated based on whole-building energy use, incorporating the combined effects of all building envelope elements and systems. However, this holistic approach may dilute the true impact of window performance improvements. A more precise evaluation can be obtained by isolating the energy performance of the window components themselves. Figure 8 presents solar heat gains and total heat losses through window components for each window type across different climate conditions. The results show that photothermal windows significantly reduce heat loss by 34.9–40.8% compared to baseline clear

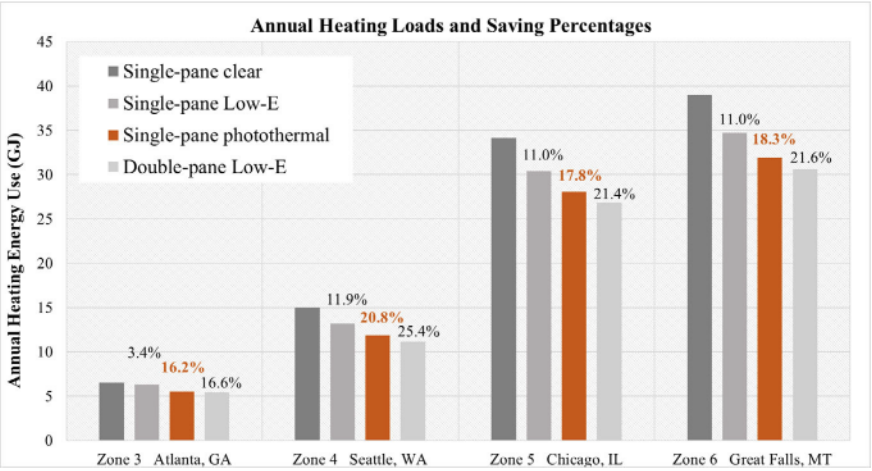

Fig. 7 Annual heating loads and associated savings percentages based on clear single-pane

single-pane windows. Additionally, when compared to low-e windows, photothermal windows still achieved 12.2–20.1% lower heat loss. The solar heat gain performance of photothermal windows also aligns with this observation. While the transmitted solar radiation levels of low-e and photothermal windows remain nearly identical, the PPE-enhanced inward-flowing heat effect in photothermal windows resulted in 14.2–16.7% greater solar heat gain than low-e windows. The combination of reduced heat loss and enhanced solar heat gain is responsible for the superior energy savings of nanoscale PPE-induced windows, making them a promising alternative for improving building energy efficiency.

3.5 Discussion of Numerical Analysis and Findings

This case study explored the energy-saving potential of surface plasmon-induced NP photothermal effects applied to single-pane windows—a solution aimed at addressing energy inefficiencies in building retrofits. While previous research has investigated the feasibility of photothermal coatings for windows, a comprehensive energy analysis has not been conducted until now. To bridge this gap, a simplified analytical model was developed to account for localized surface heating on one side of the glass pane. This model incorporated interfacial insulation effects and was validated through photothermal experiments. The validated model enabled the computation of temperature distributions under various design and environmental conditions.

Using this framework, the study analyzed the thermal performance improvements of photothermal windows compared to Low-E single-pane windows. The research focused on the dynamic Solar Heat Gain Coefficient (SHGC), specifically introducing

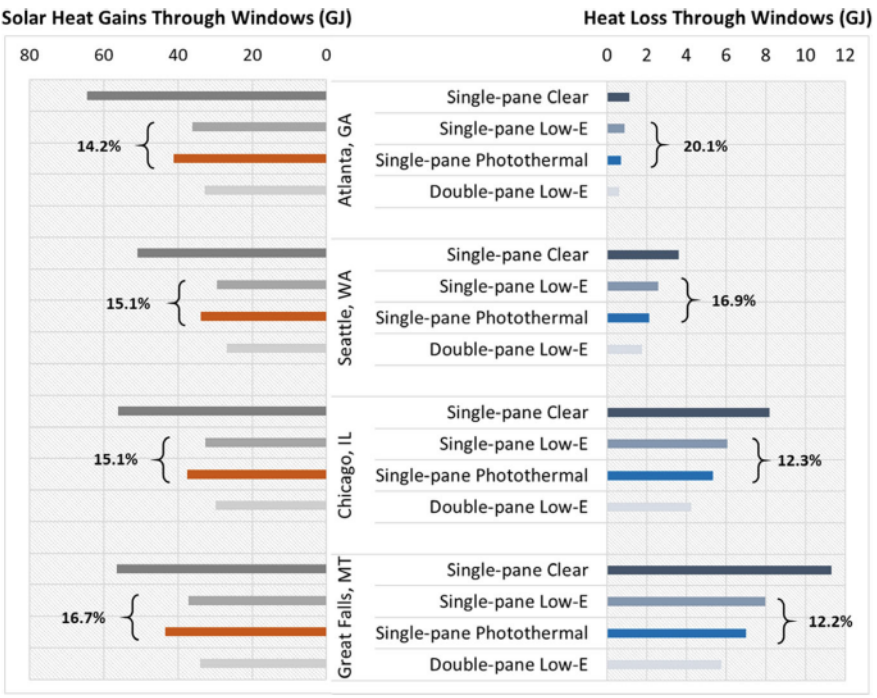

Fig. 8 Solar heat gains and building heat loss through windows

$SHGC_{PPE}$ to quantify the plasmonic photothermal effect. A physics-based mathematical model was developed through numerical analysis across multiple boundary conditions (solar irradiance levels and outdoor temperatures).

To assess the whole-building energy performance, a parametric energy simulation approach was employed, integrating the temperature- and solar-dependent SHGC. The results demonstrated that photothermal coatings offer a highly efficient energy retrofit solution for single-pane windows, achieving:

- 16.2–20.8% overall energy savings relative to single-pane clear windows.
- 12.2–21.9% reduction in heat loss compared to low-e single-pane windows.
- 14.2–16.7% greater solar heat gain due to enhanced plasmonic photothermal effects.
- 7.6–13.2% whole-building heating energy savings, making performance comparable to double-pane windows.

Unlike traditional energy-saving window technologies that rely on added insulation layers (e.g., air gaps in double-pane windows), the energy efficiency of photothermal windows is driven by nanoparticle-induced LSPR and solar NIR energy absorption. This method improves thermal performance without compromising visible transmittance (VT), making it a viable alternative to double-pane systems. Additionally, this new nanomaterial-embedded window system could offer comfort

and condensation control benefits over low-e coated single panes, addressing local thermal discomfort issues often associated with low-emissivity coatings. Considering lighting energy use, photothermal windows further narrow the performance gap with double-pane windows, offering a promising retrofit solution for enhancing solar energy utilization in buildings.

4 Summary

In the ongoing effort to enhance building energy efficiency, integrating nanoscale materials into architectural applications presents a groundbreaking opportunity. Nanomaterials, with their distinctive optical, thermal, and phase-changing properties, offer promising solutions for improving insulation, solar control, and energy retention. However, the transition from nanoscale properties to full-building performance remains complex, requiring sophisticated numerical methods to model interactions across multiple scales accurately.

This chapter systematically examines the computational frameworks necessary to bridge this gap. Molecular dynamics (MD) simulations allow for detailed analysis of thermal conductivity, phase transitions, and radiative properties at the atomic level. Finite element analysis (FEA) extends this understanding to the material component scale, helping predict how nano-enhanced materials affect the performance of building envelopes. Computational fluid dynamics (CFD) further refines the analysis by modeling heat transfer and airflow interactions within built environments. Recently, machine learning techniques, such as Physics-Informed Neural Networks (PINNs), have emerged as powerful tools for improving numerical accuracy while reducing computational costs.

A key focus of this chapter is the application of numerical simulations to solar-responsive nanomaterials in glazing systems. Windows account for a significant portion of a building's energy loss, and spectrally selective nanocoatings have the potential to modulate solar heat gain while maintaining transparency. The chapter presents a case study on localized surface plasmon resonance (LSPR)-induced photothermal effects in nanoparticle-coated glazing systems. By analyzing nanoparticle absorption, heat transfer mechanisms, and optical modulation, the study develops a physics-based numerical model that is then integrated into whole-building parametric energy simulations using EnergyPlus.

Results from the case study reveal that LSPR-mediated nanocoatings can enhance passive solar heat gain in colder climates while maintaining transparency, effectively reducing heating loads by up to 20% compared to traditional single-pane windows. These nano-enhanced windows demonstrate comparable performance to double-pane glazing, providing an alternative energy retrofit solution that avoids the added weight, cost, and installation complexity of conventional insulating glass units.

Beyond the immediate case study, this chapter underscores a broader message: numerical modeling is essential for translating nanoscale material innovations into

practical building applications. The methodologies discussed—ranging from molecular simulations to full-building energy analysis—demonstrate how multi-scale numerical approaches enable precise performance assessments before large-scale implementation. The findings contribute to the growing body of knowledge on nano-integrated architectural solutions, helping pave the way for sustainable, high-performance building materials through computational optimization. By leveraging numerical simulations, researchers and engineers can predict, optimize, and implement nano-enhanced materials in energy-efficient buildings, ensuring that these advancements move beyond laboratory studies to real-world impact in architectural engineering and urban sustainability.

Acknowledgements We acknowledge the financial support from National Science Foundation #1953004 and #2001207.

Competing Interests The author has no conflicts of interest to declare that are relevant to the content of this chapter.

References

1. Bao H, Chen J, Gu X, Cao B (2018) A review of simulation methods in micro/nanoscale heat conduction. ES Energy Environ 1:16–55
2. Arasteh H, Maref W, Saber HH (2024) 3D numerical modeling to assess the energy performance of solid–solid phase change materials in glazing systems. Energies 17(15)
3. Mastino C, Concu G, Frattolillo A (2024) Energetic performance of natural building materials: numerical simulation and experimental evaluation. Energies 17(768)
4. Duan Q, Wang J (2019) A parametric study of the combined effects of window property and air vent placement. Indoor Built Environ 28(3)
5. Zhou Y, Zheng S (2024) A co-simulated material-component-system-district framework for climate-adaption and sustainability transition. Renew Sustain Energy Rev 192
6. Liu B, Wang Y, Rabczuk T, Olofsson T, Lu W (2024) Multi-scale modeling in thermal conductivity of polyurethane incorporated with phase change materials using physics-informed neural networks. Renew Energy 220
7. Mi R, Li T, Dalgo D, Chen C, Kuang Y, He S, Zhao X, Xie W, Gan W, Zhu J, Srebric J, Yang R, Hu L (2020) A clear, strong, and thermally insulated transparent wood for energy efficient windows. Adv Funct Mater 30(1)
8. Song Y, Duan Q, Feng Y, Zhang E, Wang J, Niu S (2020) Solar infrared radiation towards building energy efficiency: measurement, data, and modeling. Environ Rev 28(4):457–465
9. Huang X, Neretina S, El-Sayed MA (2009) Gold nanorods: from synthesis and properties to biological and biomedical applications. Adv Mater 21(48):4880–4910
10. Abendroth T, Schumm B, Alajlan SA, Almogbel AM, Mäder G, Härtel P, Althues H, Kaskel S (2017) Optical and thermal properties of transparent infrared blocking antimony doped tin oxide thin films. Thin Solid Films 624:152–159
11. Liu H, Zeng X, Kong X, Bian S, Chen J (2012) A simple two-step method to fabricate highly transparent ITO/polymer nanocomposite films. Appl Surf Sci 258(22):8564–8569
12. Xu X, Stevens M, Cortie MB (2004) In situ precipitation of gold nanoparticles onto glass for potential architectural applications. Chem Mater 16(11):2259–2266
13. Xiao L, Su Y, Ran J, Liu Y, Qiu W, Wu J, Lu F, Shao F, Tang D, Peng P (2016) First-principles prediction of solar radiation shielding performance for transparent windows of GdB. J Appl Phys 119(16)

14. Schelm S, Smith GB (2003) Dilute LaB6 nanoparticles in polymer as optimized clear solar control glazing. Appl Phys Lett 82(24)
15. Hou H, Wang P, Zhang J, Li C, Jin Y (2015) Graphene oxide-supported Ag nanoplates as LSPR tunable and reproducible substrates for SERS applications with optimized sensitivity. ACS Appl Mater Interfaces 7(32):18038–18045
16. Pallavicini P, Chirico G, Collini M, Dacarro G, Donà A, D'Alfonso L, Falqui A, Diaz-Fernandez Y, Freddi S, Garofalo B, Genovese A, Sironi L, Taglietti A (2011) Synthesis of branched Au nanoparticles with tunable near-infrared LSPR using a zwitterionic surfactant. Chem Commun 47(4):1315–1317
17. Nehl CL, Hafner JH (2008) Shape-dependent plasmon resonances of gold nanoparticles. J Mater Chem 18:2415–2419
18. Jana NR, Gearheart L, Murphy CJ (2001) Seed-mediated growth approach for shape-controlled synthesis of spheroidal and rod-like gold nanoparticles using a surfactant template. Adv Mater 13(18):1389–1393
19. Garcia G, Buonsanti R, Llordes A, Runnerstrom EL, Bergerud A, Milliron DJ (2013) Near-infrared spectrally selective plasmonic electrochromic thin films. Adv Opt Mater 1(3):215–220
20. Mendelsberg RJ, Garcia G, Milliron DJ (2012) Extracting reliable electronic properties from transmission spectra of indium tin oxide thin films and nanocrystal films by careful application of the Drude theory. J Appl Phys 111
21. Khandelwal H, Loonen RCGM, Hensen JLM, Debije MG, Schenning APHJ (2015) Electrically switchable polymer stabilised broadband infrared reflectors and their potential as smart windows for energy saving in buildings. Sci Rep 3
22. Li Y, Liu J, Liang J, Yu X, Li D (2015) Tunable solar-heat shielding property of transparent films based on mesoporous Sb-doped SnO_2 microspheres. ACS Appl Mater Interfaces 7(12):6574–6583
23. Xu X, Cortie MB, Stevens M (2005) Effect of glass pre-treatment on the nucleation of semi-transparent gold coatings. Mater Chem Phys 94(2–3):266–274
24. Pardiñas-Blanco I, Hoppe CE, Piñeiro-Redondo Y, López-Quintela MA, Rivas J (2008) Formation of gold branched plates in diluted solutions of poly(vinylpyrrolidone) and their use for the fabrication of near-infrared-absorbing films and coatings. Langmuir ACS J Surf Colloids 24(3):983–990
25. Besteiro LV, Kong X-T, Wang Z, Rosei F, Govorov AO (2018) Plasmonic glasses and films based on alternative inexpensive materials for blocking infrared radiation. Nano Lett 18(5):3147–3156
26. Zhao Y, Sadat M, Dunn A, Xu H, Chen C-H, Nakasuga W, Ewing RC, Shi D (2017) Photothermal effect on Fe_3O_4 nanoparticles irradiated by white-light for energy-efficient window applications. Sol Energy Mater Sol Cells 161:247–254
27. Khashan S, Dagher S, Omari SA, Tit N, Elnajjar E, Mathew B, Hilal-Alnaqbi A (2017) Photothermal characteristics of water-based Fe_3O_4@SiO_2 nanofluid for solar-thermal applications. Mater Res Express 4
28. Wang J, Shi D (2017) Spectral selective and photothermal nano structured thin films for energy efficient windows. Appl Energy 208:83–96
29. Korpela SA, Lee Y, Drummond JE (1982) Heat transfer through a double pane window. ASME J Heat Mass Transf 104(3):539–544
30. Rubin M (1982) Calculating heat transfer through windows. Int J Energy Res
31. Siegel R, Howell JR (2002) Thermal radiation heat transfer
32. Carli I (2006) Technical report: Tarcog: mathematical models for calculation of thermal performance of glazing systems with or without shades. Technology
33. Lü X, Lu T, Viljanen M (2006) A new analytical method to simulate heat transfer process in building. Appl Therm Eng 26(16):1901–1909
34. Cuevas C, Fissore A, Fonseca N (2010) Natural convection at an indoor glazing surface with different window blinds. Energy Build 42(10):1685–1691
35. Abel E (1994) Low-energy buildings. Energy Build 21(3):169–174

36. Aydın O (2006) Conjugate heat transfer analysis of double pane windows. Build Environ 41(2):109–116
37. Littlefair P (1982) Effective glass transmission factors under a CIE sky. Light Res Technol 14(4):232–235
38. Kreith F, Bohn M, Kirkpatrick A (1997) Principles of heat transfer. J Solar Energy Eng 119(2)
39. Modest MF (2013) Radiative heat transfer
40. Arıcı M, Karabay H, Kan M (2015) Flow and heat transfer in double, triple and quadruple pane windows. Energy Build 86:394–402
41. Qiu T, Tien C (1994) Femtosecond laser heating of multi-layer metals—I. Analysis. Int J Heat Mass Transf 37(17):2789–2797
42. Qiu T, Juhasz T, Suarez C, Bron W, Tien C (1994) Femtosecond laser heating of multi-layer metals—II. Experiments. Int J Heat Mass Transf 37(17):2799–2808
43. Tzou DY (1990) Three dimensional structures of the thermal shock waves around a rapidly moving heat source. Int J Eng Sci 28(10):1003–1017
44. Majumdar A (1993) Microscale heat conduction in dielectric thin films. J Heat Transfer 115(1):7–16
45. Keith Roper D, Ahn W, Hoepfner M (2007) Microscale heat transfer transduced by surface Plasmon resonant gold nanoparticles. J Phys Chem C 111(9):3636–3641
46. Govorov AO, Richardson HH (2007) Generating heat with metal nanoparticles. NanoToday 2(1):30–38
47. Tzou D (1995) Experimental support for the lagging behavior in heat propagation. J Thermophys Heat Transf 686–693
48. Tang D, Araki N (1999) Wavy, wavelike, diffusive thermal responses of finite rigid slabs to high-speed heating of laser-pulses. Int J Heat Mass Transf 42(5):855–860
49. Ho J-R, Kuo C-P, Jiaung W-S (2003) Study of heat transfer in multilayered structure within the framework of dual-phase-lag heat conduction model using lattice Boltzmann method. Int J Heat Mass Transf 46(1):55–69
50. Huld T, Paietta E, Zangheri P, Pinedo Pascua I (2018) Assembling typical meteorological year data sets for building energy performance using reanalysis and satellite-based data. Atmosphere 9(53)
51. Lorenz E, Hurka J, Karampela G, Heinemann D, Beyer H, Schneider M (2008) Qualified forecast of ensemble power production by spatially dispersed grid-connected PV systems. In: 23rd European photovoltaic solar energy conference
52. Rabl A (1976) Comparison of solar concentrators. Sol Energy 18(2):93–111
53. Bacher P, Madsen H, Aalborg Nielsen H (2009) Online short-term solar power forecasting. Solar Energy 83(10):1772–1783
54. Roberts JE (1995) Visible light induced changes in the immune response through an eye-brain mechanism (photoneuroimmunology). J Photochem Photobiol B 29(1):3–15
55. Wang N, Wang J (2021) A spectrally-resolved method for evaluating the solar effect on user thermal comfort in the near-window zone. Build Environ 202
56. Jahid MA, Wang J, Zhang E, Duan Q, Feng Y (2022) Energy savings potential of reversible photothermal windows with near infrared-selective plasmonic nanofilms. Energy Convers Manag 263
57. Zhang E, Duan Q, Wang J, Zhao Y, Feng Y (2021) Experimental and numerical analysis of the energy performance of building windows with solar NIR-driven plasmonic photothermal effects. Energy Convers Manag 245
58. Pu J, Shen C, Wang J, Zhang Y, Zhang C, Kalogirou SA (2023) Near-infrared absorbing glazing for energy-efficient windows: a critical review and performance assessments from the building requirements. Nano Energy 110
59. Li Y, Huang X, Sheriff HKM, Forrest SR (2023) Semitransparent organic photovoltaics for building-integrated photovoltaic applications. Nat Rev Mater 8(3)
60. Du W-C, Xie J, Xia L, Liu Y-J, Yang H-W, Zhang Y (2021) Study of new solar film based on near-infrared shielding. J Photochem Photobiol A Chem 418

61. Gao Q, Wu X, Huang T (2021) Novel energy efficient window coatings based on In doped CuS nanocrystals with enhanced NIR shielding performance. Sol Energy 220:1–7
62. Xu Q, Xiao L, Ran J, Tursun R, Zhou G, Deng L, Tang D, Shu Q, Qin J, Lu G, Peng P (2018) Cs0.33WO3 as a high-performance transparent solar radiation shielding material for windows. J Appl Phys 124
63. Duan Q, Feng Y, Wang J (2021) Clustering of visible and infrared solar irradiance for solar architecture design and analysis. Renew Energy 668–677
64. Chen C, Duan Q, Feng Y, Wang J, Ghaeili Ardabili N, Wang N, Hosseini SM, Shen C (2023) Reconstruction of narrowband solar radiation for enhanced spectral selectivity in building-integrated solar energy simulations. Renew Energy 219
65. Perino M, Serra V (2015) Switching from static to adaptable and dynamic building envelopes: a paradigm shift for the energy efficiency in buildings. Eng Environ Sci
66. Fox M (ed) (2016) Interactive architecture: adaptive world. Chronicle Books
67. Moloney J (2011) Designing kinetics for architectural facades: state change. Routledge, London
68. Kolarevic B (2003) Architecture in the digital age-design and manufacturing. Spon Press, London, New York
69. Oxman R (2008) Digital architecture as a challenge for design pedagogy: theory, knowledge, models and medium. Des Stud 29(2):99–120
70. McCormack J, Dorin A, Innocent T (2004) Generative design: a paradigm for design research. In: Futureground—DRS international conference, Melbourne
71. Baetens R, Jelle BP, Thue JV, Tenpierik MJ, Grynning S, Uvsløkk S, Gustavsen A (2010) Vacuum insulation panels for building applications: a review and beyond. Energy Build 42(2):147–172
72. Alam M, Singh H, Limbachiya M (2011) Vacuum Insulation Panels (VIPs) for building construction industry—a review of the contemporary developments and future directions. Appl Energy 88(11):3592–3602
73. Baetens R, Jelle BP, Gustavsen A, Grynning S (2010) Gas-filled panels for building applications: a state-of-the-art review. Energy Build 42(11):1969–1975
74. Griffith BT, Arashteh D, Türler D (1995) Gas-filled panels: an update on applications in the building thermal envelope superinsulations and the building envelope. In: BETEC Fall symposium
75. Kuznik F, David D, Johannes K, Roux J-J (2011) A review on phase change materials integrated in building walls. Renew Sustain Energy Rev 15(1):379–391
76. Loonen R, Trčka M, Cóstola D, Hensen J (2013) Climate adaptive building shells: state-of-the-art and future challenges. Renew Sustain Energy Rev 25:483–493
77. Baetens R, Jelle BP, Gustavsen A (2010) Properties, requirements and possibilities of smart windows for dynamic daylight and solar energy control in buildings: a state-of-the-art review. Sol Energy Mater Sol Cells 94(2):87–105
78. Addington M, Schodek D (2012) Smart materials and technologies in architecture: for the architecture and design professions. Routledge
79. Wang Y, Runnerstrom EL, Milliron DJ (2016) Switchable materials for smart windows. Annu Rev Chem Biomol Eng 7:283–304
80. . Wang J, Beltran L, Kim J (2014) A parametric simulation study on kinetic envelopes. In: 43rd ASES national solar conference 2014, SOLAR 2014, including the 39th national passive solar conference and the 2nd meeting of young and emerging professionals in renewable energy
81. Kasinalis C, Loonen R, Cóstola D, Hensen J (2014) Framework for assessing the performance potential of seasonally adaptable facades using multi-objective optimization. Energy Build 79:106–113
82. Loonen R (2014) Bio-inspired adaptive building skins. In: Biotechnologies and biomimetics for civil engineering. Springer, pp 115–134
83. Goia F, Cascone Y (2014) The impact of an ideal dynamic building envelope on the energy performance of low energy office buildings. Energy Procedia 58:185–192

84. Goia F, Haase M, Perino M (2013) Optimizing the configuration of a façade module for office buildings by means of integrated thermal and lighting simulations in a total energy perspective. Appl Energy 108:515–527
85. Favoino F, Goia F, Perino M, Serra V (2014) Experimental assessment of the energy performance of an advanced responsive multifunctional façade module. Energy Build 68:647–659
86. Wang J, Beltran L, Kim J (2014) From static to kinetic: a review of acclimated kinetic building envelopes. In: SOLAR 2014 conference, American Solar Energy Society, San Francisco, CA
87. Wang J, Beltran L (2016) A method of energy simulation for dynamic building envelopes. In: ASHRAE and IBPSA-USA SimBuild 2016: building performance modeling conference, Salt Lake City, UT
88. Miao Z, Li J, Wang J (2011) Kinetic building envelopes for energy efficiency: modeling and products. In: 2011 international conference on green building, materials and civil engineering, GBM, Shangri-La
89. Duan Q, Zhang E, Hinkle L, Wang J (2021) Parametric energy simulation methods for solar-NIR selective glazing systems. In: 8th international building physics conference (IBPC 2021), Copenhagen
90. Duan Q, Hinkle L, Wang J, Zhang E, Memari A (2021) Condensation effects on energy performance of building window systems. Energy Rep 7:7345–7357
91. Hinkle L, Ghaeili Ardabili N, Wang J (2022) Parametric simulation of dynamic glazing system with changeable NIR response. In: Conference on sustainable development of energy, water, and environment system
92. Hinkle LE, Wang J, Brown NC (2022) Quantifying potential dynamic façade energy savings in early design using constrained optimization. Build Environ 221
93. Wang N, Ghaeili N, Wang J, Feng Y, Zhang E, Chen C (2023) Using architectural glazing systems to harness solar thermal potential for energy savings and indoor comfort. Renew Energy 219
94. Duan Q, Hinkle L, Wang J (2021) Parametric energy simulation considering the effects of condensation on glazing systems. In: 2021 ASHRAE virtual annual conference, ASHRAE 2021
95. Wang J, Beltran L (2021) Energy performances of future dynamic building envelopes. In: 3rd IBPSA-England conference BSO 2016, Newcastle
96. Ghaeili Ardabili N, Feng Y, Wang J (2023) Design and optimization of thermally responsive autonomous dynamic glazed attachment systems for building solar heat gain control. Build Simul 16:1971–1986
97. Ardabili NG, Feng Y, Wang J (2023) Design and optimization of thermally responsive autonomous dynamic glazed attachment systems for building solar heat gain control. In: Building Simulation vol 16, no. 10. Tsinghua University Press, Beijing, pp 1971–1986
98. Chen G (1996) Nonlocal and nonequilibrium heat conduction in the vicinity of nanoparticles. J Heat Transf 118(3):539–545
99. Neumann O, Urban AS, Day J, Lal S, Nordlander P, Halas NJ (2013) Solar vapor generation enabled by nanoparticles. ACS Nano 7(1):42–49
100. Tian Q, Hu J, Zhu Y, Zou R, Chen Z, Yang S, Li R, Su Q, Han Y, Liu X (2013) Sub-10 nm Fe_3O_4@$Cu_{2-x}S$ core-shell nanoparticles for dual-modal imaging and photothermal therapy. J Am Chem Soc 135(23):8571–8577